A Case Study of Surface Borehole Wall Dislocation Induced by Top-Coal Longwall Mining

Jinfeng Ju [1,2], Jialin Xu [3,*] and Jingmin Xu [4] (ID)

[1]   IoT Perception Mine Research Center, China University of Mining and Technology, Xuzhou 221008, China; jujinfeng2012@163.com
[2]   The National and Local Joint Engineering Laboratory of Internet Application Technology on Mine, Xuzhou 221008, China
[3]   State Key Laboratory of Coal Resources and Safe Mining, China University of Mining and Technology, Xuzhou 221116, China
[4]   Department of Civil Engineering, Faculty of Engineering, University of Nottingham, University Park, Nottingham NG7 2RD, UK; jingmin.xu@nottingham.ac.uk
*   Correspondence: cumtxjl@cumt.edu.cn; Tel.: +86-137-7658-3410

Abstract: Underground coal extraction causes failure and movement of overlying strata, which could also result in the dislocation of vertical surface boreholes. Investigating the correlation between the dislocation of surface boreholes and the broken of overlying strata is of great significance in deducing the mining-induced dynamic movement of overlying strata, which cannot be seen inside the 'black box'. Field measurement, laboratory experiment and theoretical analysis were employed to study the mechanism of the mining-induced dislocation of surface boreholes, and its relationship with the movement of overlying strata. Due to different deflection angles of adjacent strata, the horizontal movement of strata varies, and this contributes primarily to the dislocation of borehole wall. As the development of strata movement from the mining level towards surface, the position of borehole dislocation also occurred upwards, and the highest borehole dislocation occurred at the same position of overlying Key Stratum (KS). In other words, when a KS breaks, borehole dislocation will occur and develop from the bottom of this KS until the bottom of an upper KS. These key findings can provide a theoretical basis for deducing the mining-induced movement of overlying strata, determining the KS position and assessing the water conductivity of broken strata.

Keywords: surface borehole dislocation; strata movement; key stratum (KS); coal mining

1. Introduction

How the failure of overlying strata develops upwards from the coal seam after coal extraction is always a topic of attention in mining engineering. Using vertical surface boreholes to investigate the failure law of overlying strata in the mining process provides a way of addressing this problem [1]. In addition, this is a common engineering detective method in the research of strata movement and ground control in Chinese mining industry. Yet, the observation of a borehole can only indicate the influence of coal mining on borehole deformation, borehole failure and even borehole blockage, among others, as well as the convective change of these phenomena in the borehole. Apparently, those phenomena of deformation occurring in the borehole are closely related to the break and movement of overlying strata. For this reason, fundamental understanding on the deformation and failure of the borehole walls provides guidance to the strata movement control and furthermore the prevention of water and methane burst.

In the field of oil and gas exploitation, extensive analytical, experimental and numerical studies have been carried out on surface borehole instability [2–9]. The relevant research has focused on

areas as diverse as the mechanism and regularity of borehole failure due to pre-existing rock fractures, crustal stress, as well as soft or unconsolidated rock formations, the rock failure criteria for predicting borehole shear failure and the drilling technique and method of improving the borehole stability, etc. For example, Karatela et al. [2] indicated that the drilling-induced stresses led to the development of a yielded zone around a borehole, and when the initial rock stress ratio increased the rock blocks at the borehole wall tended to move towards the centre of the borehole. As a result, the yielded zone increased around the borehole. Furthermore, the change in fracture orientation highly influenced the formation of the yielded zone. Mavko and Jizba [3] found that the presence of poorly cemented sandstone increased the potential of borehole instability. Many downhole observation results [4,5] showed that sanding-induced cavities usually gave rise to borehole casing failures in unconsolidated sandstones. Ghajari et al. [6] improved that when the mud weight was close to the minimum principal stress, it will be helpful to the borehole stability in unstable shale formations. In the field of coal mining, however, relatively few studies have been performed on the mechanism of surface borehole deformation and failure due to underground coal mining. Based on the engineering practices of coal seam gas drainage using surface boreholes, Shen and Liu [10,11] analyzed the causes of the S-shape failure of borehole casings due to the non-uniform horizontal movement of broken overlying strata at different rock formations. They pointed out that the development of rock layer separation in overlying strata resulted in the tensile failure of borehole casings. Yet, few studies were undertaken on the dynamic failure of boreholes in the mining process and its relationship with the break and movement of overlying strata.

In order to attain the variation of surface borehole failure due to coal mining, video detection was conducted to observe the surface borehole wall failure in longwall face 8203 (LW8203). It was found that borehole blockage due to borehole dislocation occurred progressively from the bottom up with the working face advancing past the borehole. Moreover, the position of borehole blockage developed stepwise rather than continuously in this process (refer to Section 2.3 for details). It is preliminarily inferred that there should be some correlations between borehole blockage and mining-induced breakage and movement of overlying strata. However, why the borehole blockage location develops upwards discontinuously instead of continuously, and how to use the deformation and failure mechanism of boreholes to deduce the break and movement process of overlying strata? Both of these questions will be discussed in this paper.

During the geological processes, the rock strata are formed with varying physical and mechanical properties. They react differently to the underground mining. Among all the rock strata, the thick layers are dominant, which burden most of the overlying loading of the self-weight of the thinner rock layers. For easy understanding the strata movement induced by underground coal mining, the 'Key Strata (KS)' theory was proposed by Qian [12,13]. According to the theory, the stratum governing the movement of the whole or partial overburden strata is defined as the Key Stratum (KS). When a KS breaks, the part or whole of the overburden strata above KS will subside simultaneously. To be more specific, the former is defined as Sub-Key Stratum (SKS), whilst the latter is defined as Primary Key Stratum (PKS). There are possibly more than one SKS in the overburden, but only one PKS in a specific LW panel. This theory provides an important theoretical basis for studying strata movement and its impacts on borehole wall displacements. Currently, the theory has been widely employed in the area of ground pressure and strata control in underground coal mining [14–17]. Zhu [14] reasonably designed the spacing of backfilling pillar based on the burdening characteristics of the KS and its weighting limit. The movement of the overlying strata and the ground were effectively controlled. In addition, the findings were applied in two panels which was arranged under the villages and farmlands. Xuan [15] analysed the features of the stress distribution after excavation where a large area of the extremely thick igneous rock (it is the KS) was exposed, and found the reason of the dynamic disasters. Based on this, he proposed that the dynamic failure can be prevented by injecting grouts to the bedding separation beneath the extremely thick igneous rock. Given that the mining-induced

borehole deformation is closely related to the movement of overlying strata, thus the presented study will be preceded on basis of this theory.

2. Field Observation and Simulation Model Design

2.1. Geological Conditions

LW8203 is the first working face of the second panel in the No. 3–5 coal seam. The length of LW8203 is 2081.6 m and its width is 200 m. The thickness of the coal seam ranges from 11.0 m to 23.6 m with an average thickness of 14.9 m. The dip of LW8203 is in the range of 3~10°. The longwall face employed the mechanised top coal caving method with a cutting height of 3.9 m. The top coal was excavated with the caving method and the recovery rate of the top coal was approximately 70%. The longwall face employed the ZF15000/27.5/42 caving hydraulic supports which has a rated working resistance of 15,000 kN. Above the longwall face was a goaf in the Jurassic coal seam, which was 150~200 m away from the No. 3–5 coal seam.

As shown in Figure 1, a borehole 108 mm in diameter was drilled 500 m ahead of the working face during the excavation process. The borehole had a distance of 1240 m from the start-up and was in the middle along the dip. During the drilling process, coring and lithology description were conducted to obtain the stratigraphical column of the overlying strata as presented in Figure 2. The borehole was drilled until reaching the bottom of the No. 3–5 coal seam with a total depth of cover of 516.9 m. Considering the borehole section of 0~321.8 m in depth was in the broken strata induced by the excavation of the Jurassic coal seam, borehole casings were installed in the borehole section of 0~341 m in depth for protection, whereas no borehole casings were installed in the remaining section.
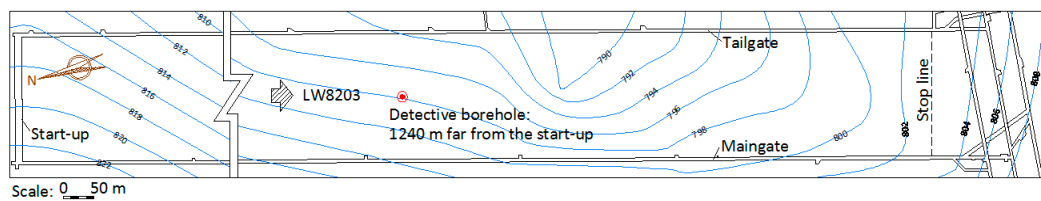

Figure 1. Layout of LW8203 top-coal caving face.

No.	Thickness/m	Depth/m	Lithology	Remark	No.	Thickness/m	Depth/m	Lithology	Remark
1	27.6	27.6	Loess		36	8.3	350.3	Silty mudstone	
2	1.7	29.3	Siltstone		37	1.2	351.5	Coarse grained sandstone	
3	35.4	64.7	Medium grained sandtone		38	8.4	359.9	Silty mudstone	
4	4.1	68.8	Fine grained sandtone		39	2.1	362.0	Medium grained sandtone	
5	20.3	89.1	Medium grained sandtone		40	23.3	385.3	Coarse grained sandstone	SKS 5
6	1.5	90.6	Coal		41	2.5	387.8	Medium grained sandtone	
7	19.2	109.8	Silty mudstone		42	2.3	390.1	Silty mudstone	
8	40.2	150.0	Fine grained sandtone	PKS	43	4.7	394.8	Medium grained sandtone	
9	3.3	153.3	Siltstone		44	3.0	397.8	Coarse grained sandstone	
10	0.8	154.1	Coal		45	8.6	406.4	Silty mudstone	SKS 4
11	0.8	154.9	Siltstone		46	1.3	407.7	Fine grained sandtone	
12	0.6	155.5	Coal		47	2.5	410.2	Medium grained sandtone	
13	34.1	189.6	Siltstone	SKS 8	48	2.6	412.8	Fine grained sandtone	
14	2.2	191.8	Coal		49	8.1	420.9	Siltstone	
15	11.9	203.7	Siltstone		50	9.6	430.5	Medium grained sandtone	SKS 3
16	4.7	208.4	Silty mudstone		51	1.9	432.4	Coarse grained sandstone	
17	1.8	210.2	Fine grained sandtone		52	0.5	432.9	Coal	
18	3.5	213.7	Siltstone		53	2.0	434.9	Silty mudstone	
19	1.5	215.2	Medium grained sandtone		54	0.7	435.6	Medium grained sandtone	
20	18.4	233.6	Siltstone	SKS 7	55	4.8	440.4	Siltstone	
21	2.2	235.8	Coarse grained sandstone		56	1.9	442.3	Coarse grained sandstone	
22	5.3	241.1	Siltstone		57	6.6	448.9	Siltstone	SKS 2
23	9.1	250.2	Fine grained sandtone		58	1.4	450.3	Silty mudstone	
24	6.0	256.2	Siltstone		59	1.5	451.8	Coal	
25	2.5	259.7	Coal		60	2.4	454.2	Silty mudstone	
26	2.4	262.1	Fine grained sandtone		61	3.8	458.0	Fine grained sandtone	
27	21.5	283.6	Medium grained sandtone	SKS 6	62	8.3	466.3	Sandy conglomerate	SKS 1
28	4.7	288.3	Silty mudstone		63	0.6	466.9	Coal	
29	9.9	298.2	Medium grained sandtone		64	1.9	468.8	Silty mudstone	
30	5.2	303.4	Silty mudstone		65	1.9	470.7	Coal	
31	4.0	307.4	Coal		66	4.6	475.3	Siltstone	
32	12.0	319.4	Silty mudstone		67	3.3	478.6	Coal	
33	2.4	321.8	Coal		68	2.6	481.2	Carbonaceous mudstone	
34	17.5	339.3	Silty mudstone		69	21.0	502.2	3^{-5} coal	
35	2.7	342.0	Coarse grained sandstone						

Figure 2. Stratigraphical column obtained from the detective borehole.

2.2. The Identification of KS

The thick and hard rock layers, termed as KS, play an important role in strata movement and strata control [12,13,18]. As a result, locating the KS is conducive to characterize the strata movement and its impact on surface borehole stability. According to References [12,13,19], the KS position can be determined by the following steps:

Firstly, determine the stiffness of the rock strata. The stiffness of the KS is larger than those of the others. The deformation of the KS does not comply with the below rock strata. Thus, the loading of the KS is not burdened by the rock strata below. According to this, the hard strata which is possible to be the KS can be determined starting from the coal seam upwards.

Secondly, apply the strength principle. The broken interval of the KS is larger than that of the hard strata below. As a result, the KS position can be defined by comparing the broken interval of each hard stratum. For the kth hard stratum, if the broken interval is larger than that of the $(k-1)$th hard stratum below, then this hard stratum is a KS. If not, the broken interval of the $(k-1)$th hard stratum should be re-calculated by adding the kth hard stratum's load. Then distinguishing whether the strength principle can be satisfied by the hard strata in the overburden layer by layer upwards. All the key strata can be finally determined.

Considering that it is quite complex to manually identify the KS, Xu [19] developed the software 'KSPB' to automatically locate the KS position. Take the stratigraphical column in Figure 2 for example, a new file should be built firstly. Then inputting parameters including the properties of the overlying rock strata material (Table 1, obtained by lab tests), the broken angle of the rock layers (80°) and the load transfer coefficient of loess (0.8), the positions of KS can be calculated and determined. The workflow to determine the KS of LW8203 is shown in Figure 3, the results are presented in Figure 2.

Table 1. Physico-mechanical properties of the overlying rock material of LW8203.

No.	Rock Stratum	Bulk Density γ/kN·m^{-3}	Elastic Modulus E/GPa	Tensile Strength σ_t/MPa
1	Loess	17.0	0	0
2	Silty mudstone	24.1	18.0	2.3
3	Siltstone	23.8	40.0	3.8
4	Fine grained sandstone	25.2	43.4	4.2
5	Coarse grained sandstone	25.0	39.7	3.2
6	Sandy conglomerate	24.8	38.0	2.9
7	Carbonaceous mudstone	24.0	10.0	1.3
8	Medium grained sandstone	25.2	41.2	3.8
9	Coal	13.0	3.0	2.0

(**a**)   (**b**)

Figure 3. *Cont.*

(**c**)

(**d**)
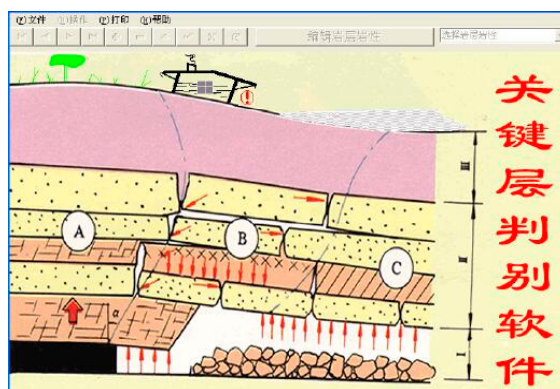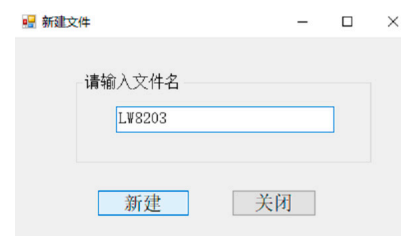
Figure 3. The workflow to determine the KS of LW8203 (Chinese version). (**a**) Software interface; (**b**) Creating a file; (**c**) Entering the properties of the overlying rock material; (**d**) Calculating and generating the diagram.

From Figure 2, it is observed that there were a total of nine KS in the overlying strata due to the large depth of the No. 3–5 coal seam. Among those KS, five KS existed between the No. 3–5 coal seam and the goaf of the Jurassic coal seam (i.e., No. 34 to No. 68 rock formations in Figure 2). Thus,

in the excavation process of the No. 3–5 coal seam, the deformation of the uncased borehole section was mainly related to the movement of SKS 1~SKS 5, whereas the deformation of the cased borehole section was primarily related to the movement of SKS 6~PKS of Jurassic strata.

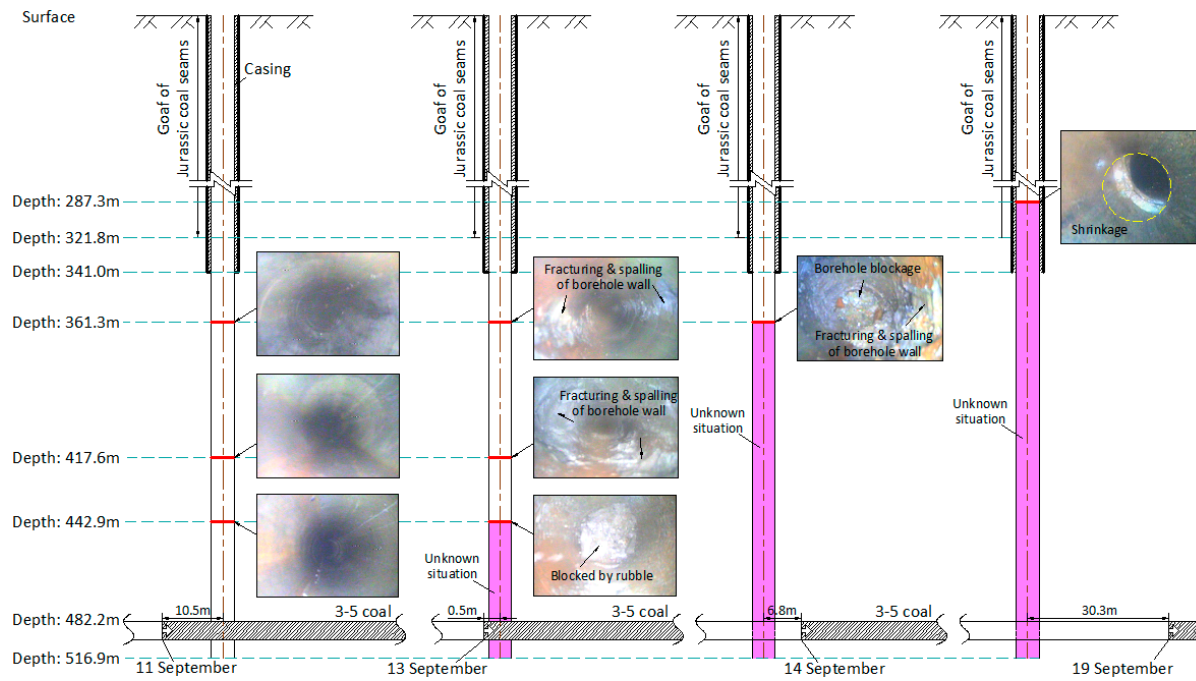## 2.3. Field Observation of the Surface Borehole Failure

In order to attain the surface borehole deformation induced by the excavation of the No. 3–5 coal seam, a high-definition observation TV (Figure 4) was employed to conduct the field observation once every one to two days. When the distance between the working face and the borehole was in the range of 10–50 m, the observation was conducted once in two days. When the distance was less than 10 m and the advancing distance was within the range of 85 m, the observation was conducted once per day. In this stage, the strata movement was extent to the range of the borehole. When the advancing distance was within the range of 85–150 m, the observation was resumed as once in two days. The observation results are given in Figure 5.

On 11 September, when the working face advanced at a distance of 10.5 m from the borehole, the borehole wall still remained smooth and the surrounding rock masses of the borehole stayed intact without noticeable fracturing or borehole wall failure. Until 13 September, when the distance from the working face to the borehole reduced to merely 0.5 m, obvious spalling of the borehole wall occurred, which resulted in the borehole blockage at the depth of 442.9 m. As a result, the observation TV could not go further down in the borehole. When the working face continued advancing past the borehole at a distance of 6.8 m (on 14 September), the spalling of the borehole wall intensified and the borehole blockage position rose to the depth of 361.3 m, as shown in Figure 5a. In the following few days (15 September to 18 September), when the working face advanced past the borehole at a distance of 13.2~26.6 m, the blockage remained at the depth of 361.3 m with water accumulation, which indicated the borehole was fully blocked at this point. Until 19 September, when the working face advanced past the borehole at a distance of 30.3 m, the borehole deformation developed upwards to the depth of 287.3 m, which led to the shrinkage of borehole casings. After that, with the working face departed further away from the borehole, the deformation of the borehole casings intensified progressively and the position of casing deformation rose gradually. To be more exact, the deformation and even dislocation of the borehole casings occurred successively at the depths of 235.6 m, 167.7 m and 131.5 m as shown in Figure 5c–f.

In light of the above analysis, it is known that when the working face advanced to and departed from the borehole, the position of borehole deformation rose in a stepwise manner irrespective of the installation of borehole casings, as shown in Figure 6. In addition, comparing the borehole deformation in Figure 6 to the stratigraphical column in Figure 2 indicates that all of the borehole deformation steps occurred in the vicinity of KS. In order to understand the mechanism of this relationship, a similarity simulation experiment was conducted in the laboratory, which is presented in Section 3 in detail.

| (**a**) | (**b**) |

Figure 4. Borehole TV and field observation of surface borehole deformation. (**a**) Borehole TV; (**b**) Field test photo.
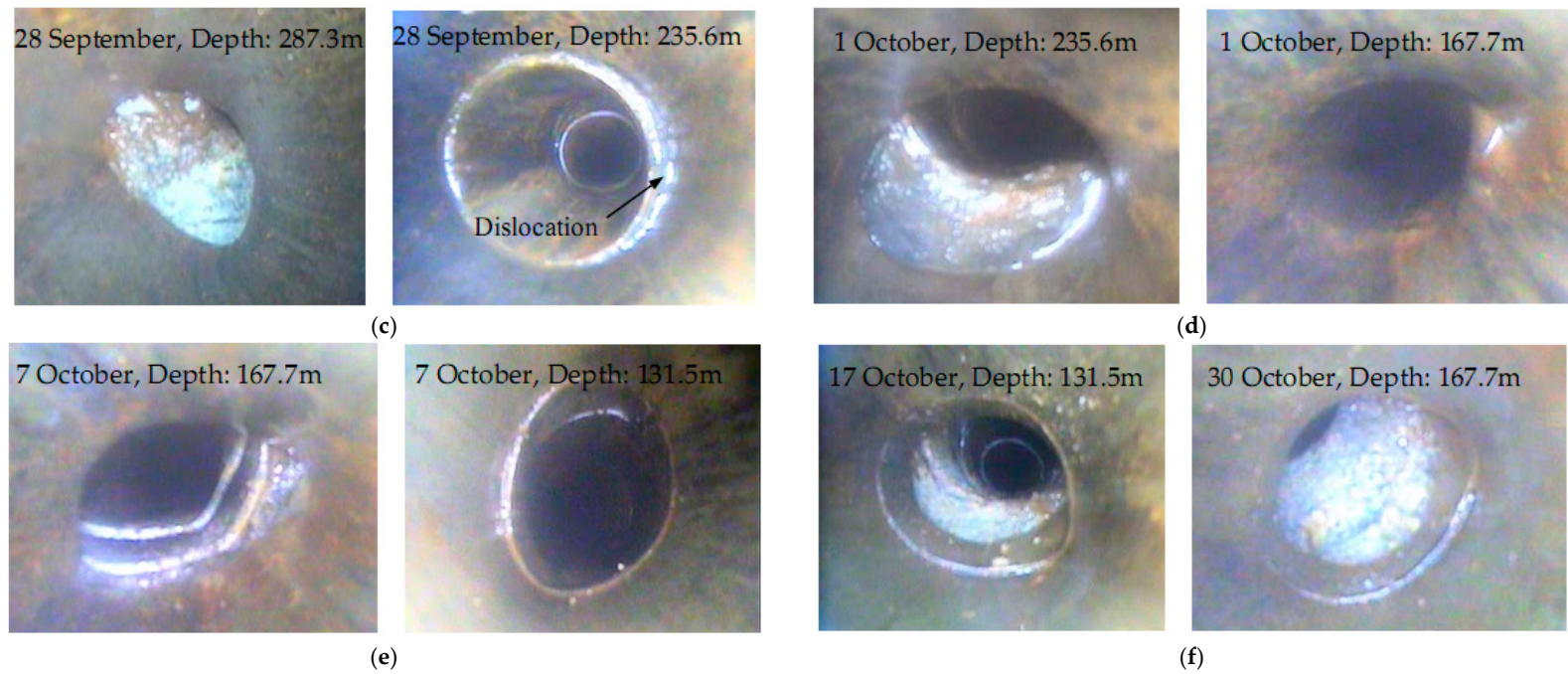
(a)
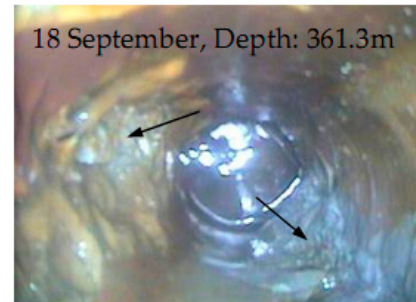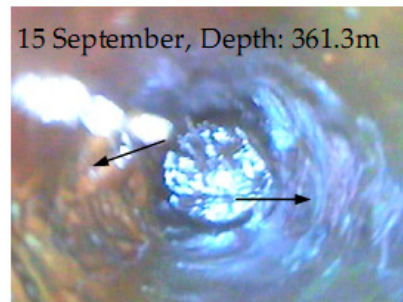
(b)

Figure 5. *Cont.*

Figure 5. Field observation results of the surface borehole deformation. (**a**) Variation of the surface borehole wall deformation with working face advancing; (**b**) Intensified spalling of borehole wall with water accumulation at the depth of 361.3 m; (**c**) Borehole deformation on 28 September; (**d**) Borehole deformation on 1 October; (**e**) Borehole deformation on 7 October; (**f**) Borehole deformation on 30 October.
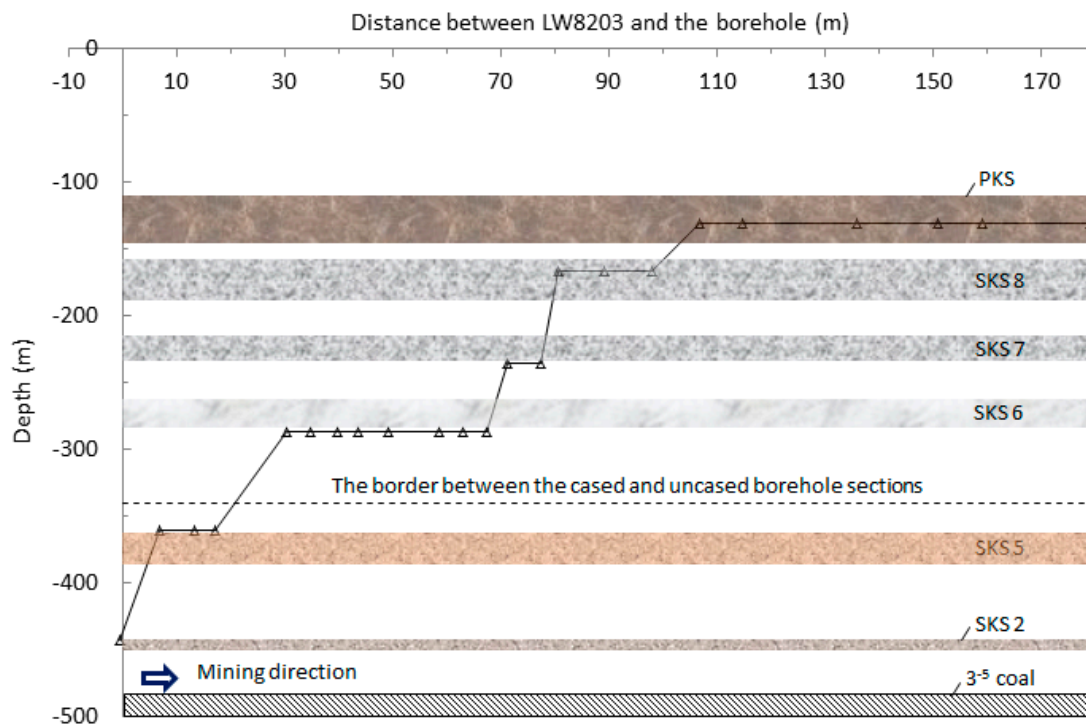
Figure 6. The relationship between the dislocation or blockage of the surface borehole and the advance of the working face.

2.4. Design of Simulation Experiment

The field observation results indicated that under the influence of coal extraction, the borehole exhibited phenomena of dislocation and blockage. In order to explore the causes of these phenomena and their relationship with the movement of the overlying strata, a similarity simulation experiment was conducted.

The experiment was conducted with a two-dimensional model frame. The model frame is 1300 mm long and 120 mm wide. The dimensional scale of the experimental model to the actual working face is 1:100 and the constant of density similarity and strength similarity are 1:1.6 and 1:160 respectively. According to the field measurements in Figure 6, the block position of the dislocated borehole is consistent with the location of the KS. Thus, it is reasonable to assume they are highly interrelated. By simplifying the mining situation of LW8203, an experimental model was employed as shown in Figure 7a, which was used to emphatically study the relationship between the movement of the KS and the dislocation of the borehole. There were three KS in the simplified model with a coal seam thickness of 40 mm (as this was a qualitative analysis, the reduction of mining height was expected to not affect the experimental result). When building up the model, three PVC pipes 20 mm in diameter were fixed in the middle of the model with spacing of 200 mm. After assembling the model, the PVC pipes were pulled out from the model to form detective boreholes which extended to the bottom of the coal seam, as shown in Figure 7b. River sand was used as aggregates, and gypsum and calcium carbonate were used as binding agent. One layer of mica was placed between rock layers to simulate the bedding and stratification in overlying strata. The thickness of all soft rock layers between two KS was 20 mm. The mixing ratio of the model materials and their weight of each simulated rock layer are presented in Table 2 as well as the physico-mechanical properties of the in-situ rock layers and corresponding simulation materials [20].

Table 2. Mixing ratio of similarity material and physico-mechanical parameters of each stratum.

| No.	Rock Strata	Thickness (m)	Material Weight (kg)	Material Ratio		Bulk Density (kN/m^3)		Elastic Modulus (GPa)		Poisson's Ratio		Cohesion (MPa)		Internal Friction Angle (°)	
				Sand:CaCO$_3$:Gypsum	Water (kg)	Prototype	Model	Prototype	Model	Prototype	Model	Prototype	Model	Prototype	Model
1	Overlying soft rock	42	98.3	50:7:3	10.9	22	15	10	0.075	0.26	0.26	4.0	0.030	33	33
2	PKS	5	11.7	30:3:7	1.3	26	15	43	0.250	0.32	0.32	12.0	0.071	40	39
3	Soft rock	28	65.5	40:7:3	7.3	23	15	10	0.075	0.26	0.26	4.0	0.030	33	33
4	SKS 2	5	11.7	40:5:5	1.3	25	15	40	0.200	0.30	0.30	9.6	0.058	36	36
5	Soft rock	20	46.8	40:7:3	5.2	23	15	10	0.075	0.26	0.26	4.0	0.030	33	33
6	SKS 1	5	11.7	40:5:5	1.3	25	15	40	0.200	0.30	0.30	9.6	0.058	36	36
7	Immediate roof	16	37.4	40:7:3	4.2	23	15	10	0.075	0.26	0.26	4.0	0.030	33	33
8	Coal	4	7.0	70:7:3	0.8	13	15	3	0.038	0.21	0.21	2.0	0.015	28	30

(a)

(b)

(c)
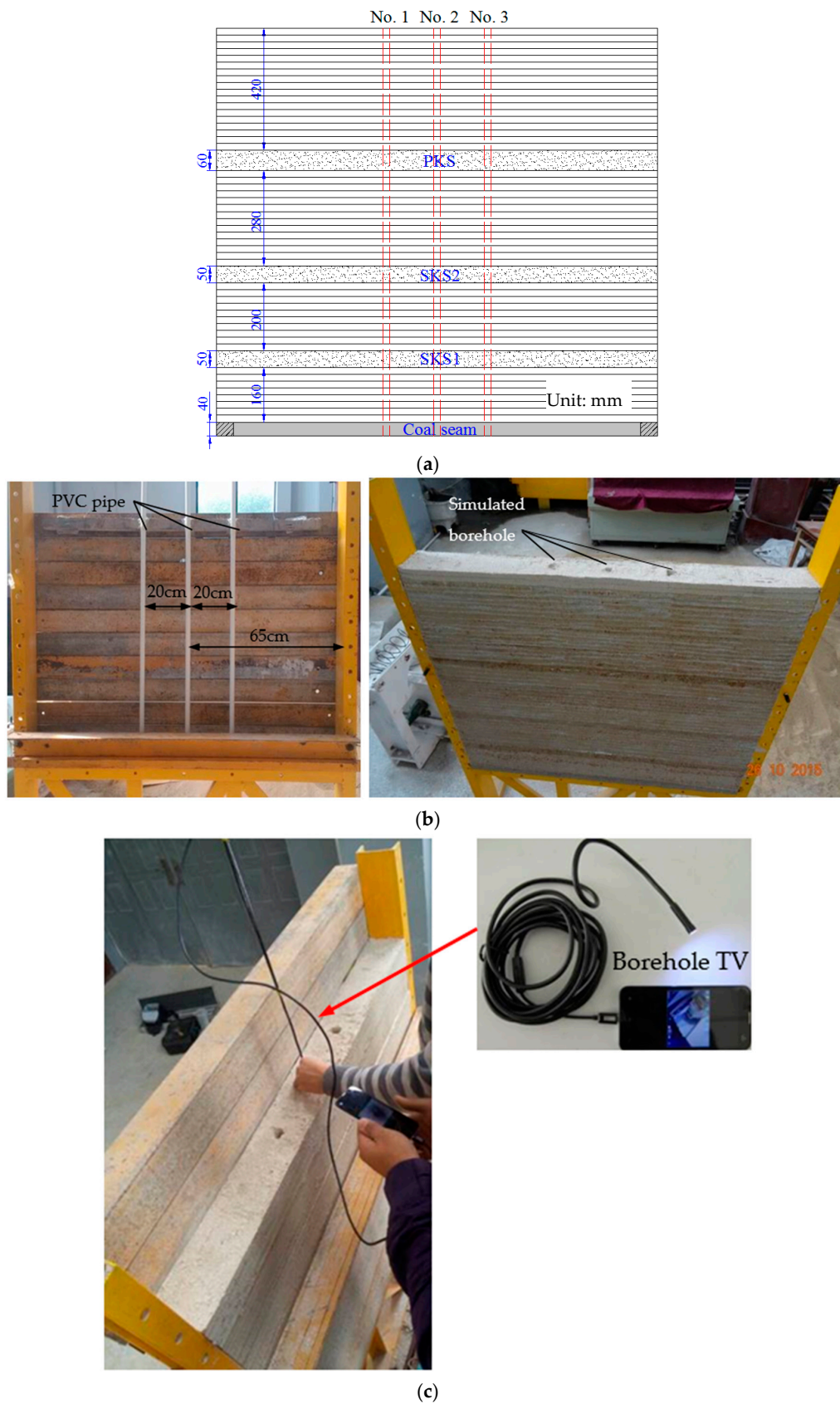
Figure 7. Simulation experiment model and borehole observation method. (**a**) Design of simulation experiment model; (**b**) Formation of the simulated borehole; (**c**) Observation method of borehole deformation.

In the mining process, the coal seam was cut off from left to right 50 mm every excavation. A 20-cm thickness protective coal pillar was set on both sides of the model. After each excavation, the borehole deformation was observed with the observation TV as shown in Figure 7c and the borehole wall deformation condition as well as the position were recorded and summarised.

3. Main Results of Similarity Simulation Experiment

As can be seen from the simulation results in A 1-1 of Figure 8a, when the working face advanced to the 1# borehole, the immediate roof around the 1# borehole broke, whereas the SKS 1 remained protruding, which resulted in the dislocation of the 1# borehole at the bottom of SKS 1. As the excavation did not affect the other area, the 1# borehole section above the SKS 1 and the other two boreholes did not experience noticeable dislocation (B 1-0 and B 2-0 of Figure 8a).

With the working face further advancing, the SKS 1 experienced its first break, which resulted in the break of all soft rock layers governed by SKS 1 (i.e., all rock layers between SKS 1 and SKS 2). The borehole observation indicated the dislocation in the 1# borehole had leaped to the bottom of SKS 2 and a stepped dislocation set emerged in the soft rock layers between SKS 1 and SKS 2 (D 1-1 of Figure 8b). As shown in Figure 8a,b, the borehole dislocation at the bottom of SKS 1 had diminished slightly (A 1-1 and A 1-2). For the 2# borehole, as the SKS 1 still stayed protruding around the 2# borehole, borehole dislocation similar to that shown in A 1-1 of Figure 8a also occurred at the bottom of SKS 1 as shown in A 2-1 of Figure 8b. However, the dislocation in the 2# borehole was apparently smaller than that in the 1# borehole due to the smaller deflection of the immediate roof around the 2# borehole.

As the working face continued advancing, SKS 2 experienced its first break and the roof movement progressed to the bottom of PKS (Figure 8c). As a result, the position of dislocation in the 1# borehole also leaped to the bottom of PKS with the presence of apparent separation of rock layers. In addition, the dislocation in the 1# borehole at the bottom of SKS 1 further diminished (A 1-1, A 1-2 and A 1-3). In the 2# borehole, as the SKS 1 and SKS 2 both experienced break, the position of dislocation in the 2# borehole also leaped to the bottom of PKS. In the 3# borehole, since the broken SKS 1 experienced merely small deflection, only fracturing and slight dislocation occurred at the bottom of SKS 1, which was similar to the previously mentioned deformation in the 2# borehole as shown in A 2-1. According to the above analysis of the dislocation at the bottom of the three KS in the 1# borehole (A 1-1, B 1-1, C 1-1), it can be concluded that the higher a KS was, the smaller the borehole dislocation at the bottom of the KS was, as given in Table 3.

Table 3. Maximum dislocation of the 1# borehole at the bottom of the three key strata (KS).

Position	Bottom of SKS 1	Bottom of SKS 2	Bottom of PKS
Maximum dislocation (mm)	8.2	4.3	2.6

Eventually, when the working face advanced past the 3# borehole at a distance of 240 mm, the PKS underwent its first break, which resulted in the break and subsidence of all the overlying strata and the presence of stepped dislocation sets in the 1# and 2# boreholes as shown in Figure 8d. As for the 3# borehole, since it was exactly located on the break line of the PKS, noticeable fractures were observed in and above the PKS and small dislocation was detected at the bottom of the PKS. In addition, as can be seen from A 1-4, as the goaf was progressively consolidated, the borehole dislocation disappeared gradually and the borehole diameter returned to its original state in the 1# borehole.
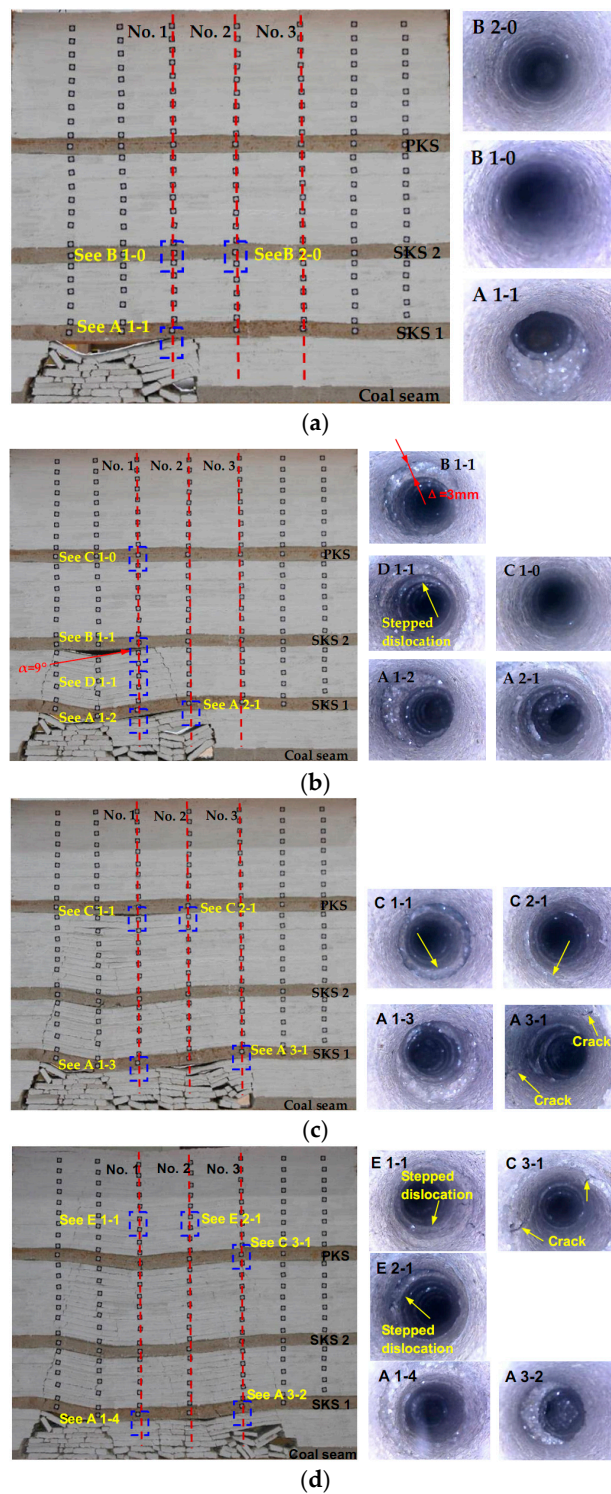
Figure 8. The observation results of the strata movement and borehole deformation with coal seam mining. (**a**) Working face advanced past the 1# borehole at a distance of 70 mm; (**b**) Working face advanced past the 2# borehole at a distance of 110 mm and the SKS 1 experienced its first breaking; (**c**) Working face advanced past the 3# borehole at a distance of 30 mm and the SKS 2 experienced its first breaking; (**d**) Working face advanced past the 3# borehole at a distance of 240 mm and the PKS experienced its first breaking.

4. Discussion

- The borehole dislocation was caused by the incompatible movement of broken adjacent rock strata. To be exact, the different horizontal rock movement due to the difference in the deflection (angle) of different rock layers was the primary cause of the borehole dislocation.

As shown in Figure 9, the borehole dislocation at the interface between the broken and unbroken rock strata is equal to the horizontal movement of the broken rock stratum due to its deflection. The larger the deflection of the broken stratum, the greater the corresponding horizontal movement and accordingly the borehole dislocation at the stratum interface. Thus, the broken rock stratum that is farther from the coal seam yielded smaller deflection, which accordingly caused smaller borehole dislocation. This was in consistence with the diminishing borehole dislocation shown in A 1-1, B 1-1 and C 1-1 in the simulation experiment (Table 3). Furthermore, for a specific rock layer, the rotation angle of the broken block increases before its subsidence maximises with the working face advancing. Thus, the borehole dislocation was increased, which was consistent with the field observation shown in Figure 5. Take the borehole dislocation at the depth of 361.3 m shown in Figure 5a,b for example, on 14 September, rock fragments crowded in the borehole while there was no sign of stagnant water, indicating the borehole was still unimpeded. However, from 15 September to 18 September, detection of immobile water inside the borehole suggested that the borehole has been blocked. The status of the borehole evidenced that it was exactly the increase of borehole dislocation and eventually full blockage that resulted in the non-water borehole on 14 September and water accumulation in the borehole during the period of 15 September to 18 September (Figure 10).

Similarly, when two adjacent strata were both broken, the borehole dislocation at the interface of these two strata was equal to the difference between their horizontal movement at the borehole. As the deflection of the upper rock stratum was always smaller than that of the lower rock stratum, the stepped borehole dislocation which diminished from bottom to top occurred in the borehole as shown in D 1-1, E 1-1, and E 2-1 in Figure 8.
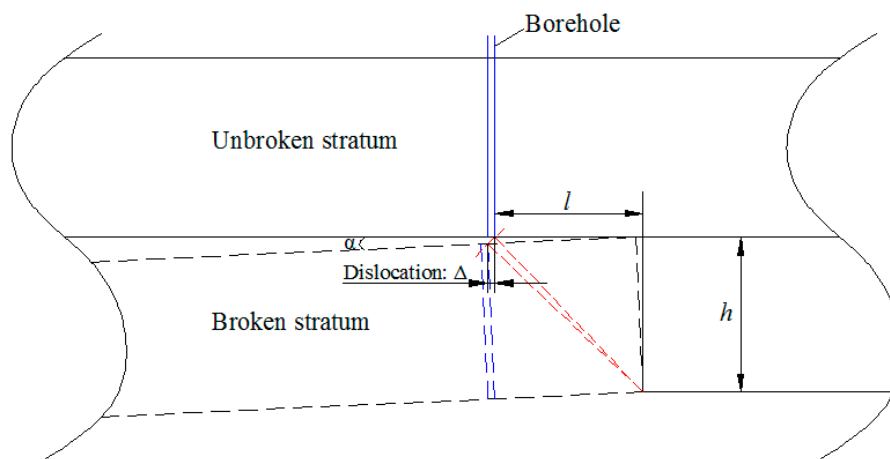

Figure 9. Schematic diagram of the borehole dislocation induced by the deflection of broken strata.
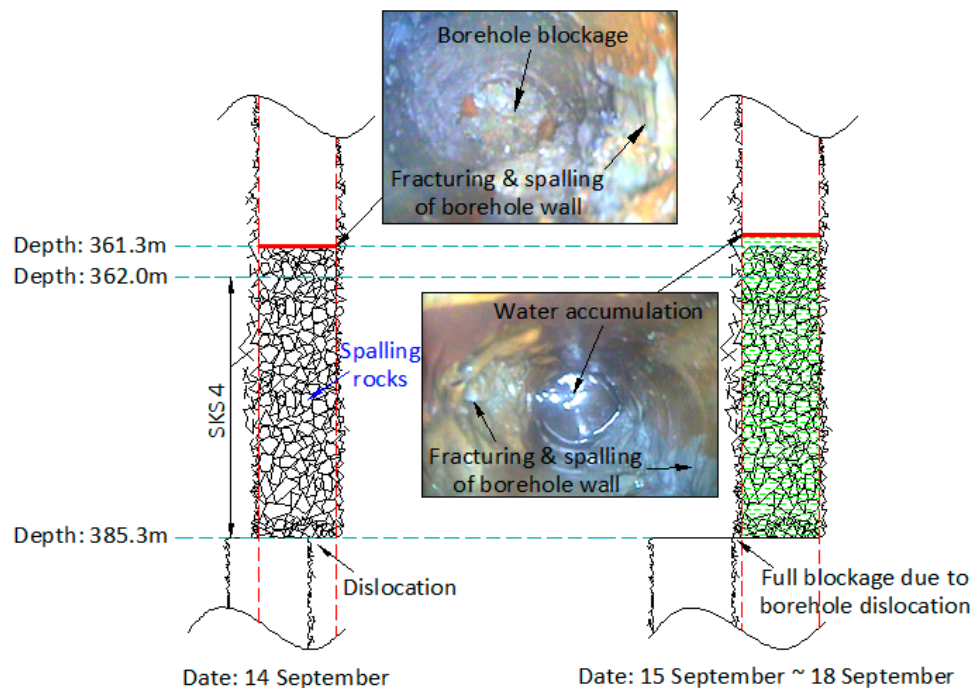
Figure 10. Schematic of water accumulation in the borehole at the depth of 361.3 m.

- The position of borehole dislocation rose in a stepwise manner with the break of overlying strata, the latest dislocation position corresponded to the bottom of KS.

When a particular KS broke, the rock layers governed by this KS (i.e., the rock layers between this KS and an upper adjacent KS) broke as well, which resulted in the borehole dislocation jumping from the bottom of the broken KS to the bottom of the upper adjacent unbroken KS. In the other words, if the borehole dislocation remained still at a particular depth (the horizontally linear stages in Figure 6), it can be inferred that this position was at the bottom of a KS which was unbroken and protruding. In the same manner, when the break of all KS developed from bottom to top, the borehole dislocation rose in a stepwise manner accordingly. This reasonably explains the field observation results shown in Figure 6 that the borehole dislocation or blockage was located in the vicinity of KS and rose in a stepwise manner. According to those above, the breakage movement of the overlying strata and its influential range can be determined by the position of the dislocation of the borehole. That is to say, at the position where borehole wall dislocation occurs, the rock layer in corresponding level has broken.

It is worth noting that the observed borehole blockage near the position of the SKS 2 and SKS 5 was located at the top of both SKS, which was slightly different from the above analysis that the borehole blockage was located at the SKS bottom. Considering the spalling of borehole wall and the accumulation of broken rocks at the position of borehole blockage, it can be inferred that this difference was caused by the accumulation of the spalling rocks as shown in Figure 10. That is to say, the borehole dislocation still occurred at the bottom of the SKS, whereas the borehole blockage progressed to the top of the SKS due to the accumulation of the spalling rocks.

- With both of the positive and negative deflection of overlying strata the borehole dislocation increased first and then decreased until the aperture returning to the original state.

Figure 11 schematically shows the deflection process of a broken stratum. When the stratum breaks, a rock block I will form at the position of break. With the increase of the block I deflection, the borehole dislocation increases progressively, reaching a maximum when the block I stopped

deflecting in the positive direction. Then with the further advance of the working face, the stratum will experience its second break and another rock block II forms. When the block II starts deflecting the block I will be reversed, which results in the horizontal movement of the block I in the opposite direction. As a result, the borehole dislocation diminishes until the aperture returning to the original state when the block I is reversed to the horizontal state. This schematic deflection process is consistent with that presented in A 1-1~A 1-4.

This finding can be very useful in practice for designing reasonable surface borehole locations, especially in the condition that requires higher borehole through flow capacities. If boreholes are located near the mining panel boundary, the through flow capacity will be limited. This is due to the borehole blockage caused by the only possible way of positive rotation after strata breakage. However, if the boreholes are located near the middle part of the mining panel, the dislocated borehole wall can be restored to its original state because after the positive rotation the broken strata will be reversely rotated back. This is beneficial to the borehole through flow capacity. The above mentioned agrees well with the physical simulation in Figure 8d. The borehole dislocations are different at the same level of borehole No. 1 in the middle section of the mining area and borehole No. 3 in the boundary area of the mining area.
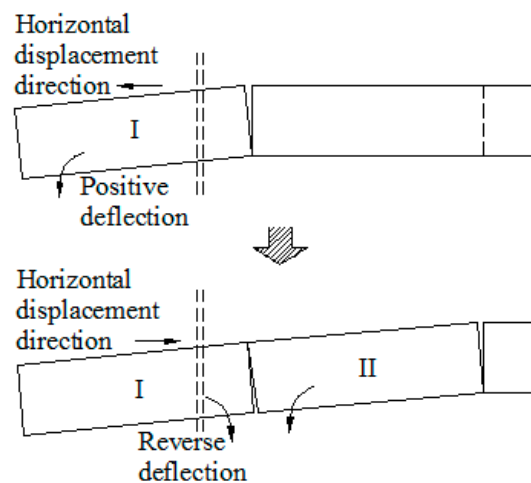

Figure 11. Schematic process of the breaking and deflection of a rock stratum.

- The borehole dislocation can be used to assess the aperture of broken strata and its water conductivity.

As shown in Figure 9, according to the geometrical relationship the borehole dislocation Δ, can be obtained as follows:

$$\Delta = l\,(\cos\alpha - 1) + h\,\tan\alpha, \tag{1}$$

where: h is the thickness of the broken stratum; α is the deflection angle of the broken stratum and l is the distance from the break line of the stratum to the borehole. From Equation (1), it can be seen that the borehole dislocation is primarily related to the deflection angle of the broken stratum, the thickness of the broken stratum and the distance from the break line to the borehole. To be exact, the borehole dislocation has a positive relation with h and α, whilst it is in a negative relation with l. Thus, Equation (1) can be validated against the results of the physical experiments in Figure 8. Take borehole 1# that dislocated at the end interface of the SKS 2 (B 1-1 of Figure 8b) for example, experimental measurement suggested the thickness of the broken stratum was 20 mm with rotation angle (α) of 9°. The distance l between borehole 1# and the line of the broken stratum was 40 mm. Thus, the right part of Equation (1) equals 2.7 mm, approximating the dislocation of the borehole wall of Δ = 3 mm. The strong agreement between analytical and experimental results demonstrated the confidence of the proposed Equation (1).

Given the deflection angle α is small, the component of Equation (1), $l(\cos\alpha - 1)$, is negligible. Thus, Equation (1) can be simplified as follows:

$$\Delta = h\tan\alpha. \tag{2}$$

Therefore, the rotation angle of the broken stratum can be determined based on the dislocation of the borehole wall. The opening and conductivity of the fissures highly depends on the rotation angle of the broken stratum; hence, the observed borehole dislocation can be used to estimate the aperture and to assess the water conductivity of the broken stratum.

The degree of fissure trace of the broken stratum, which is ratio between the length of the fissure and the thickness of the stratum, can be expressed as [21]:

$$D = 1 - \frac{\delta}{hr_p\,\alpha}, \tag{3}$$

where, δ is the limiting opening of the fissure edge, r_p is the plastic rotation factor; when D reaches 0.9–1.0, it is suggested that the fissure is conductive and the stratum is located within the water conductivity fracture zone. Therefore, whether the fissure is conductive or not can be examined by the dislocation of the borehole wall according to Equations (2) and (3).

Take the dislocation of the borehole wall at depth 361.3 m in Figure 5b for instance, the dislocation should result from the rotation of the 2.5-m-thick medium grained sandstone located at the bottom interface of SKS 5. The minimal dislocation of the borehole wall, Δ is estimated as the borehole diameter of 108 mm, then the rotation angle is no less than 2.5° according to Equation (2). Thus, D minimizes at 0.94 since δ is roughly equal to 3 mm and r_p is 0.46 [21]. Consequently, the fissures must be conductive. This agrees with the observation that the water inside the Jurassic gob flooded into the working face. Therefore, examining the conductivity of the fissures after stratum breakage based on the borehole wall dislocation is feasible with high accuracy.

5. Conclusions

- Due to the break and movement of the overlying strata, dislocation is likely to occur in the detective surface borehole. The relationship between the position of borehole dislocation and the advance distance of a working face showed a step-like pattern. The platforms of step correspond to the KS positions, indicating the break and movement of the rock strata is controlled by KS. Therefore, the dynamic dislocation of surface borehole can be used to determine KS positions in the overburden.

- The borehole dislocation is caused by different horizontal rock movement due to the deflection difference of adjacent rock strata. The bigger the difference in the deflection of adjacent strata, the larger the borehole dislocation at the interface between adjacent strata. Therefore, the broken rock stratum farther from the coal seam will yield smaller deflection, resulting in smaller borehole dislocation. Thus, the mathematic expression between the rotation angle and the borehole wall dislocation can be derived. Meanwhile, this expression has been verified by data obtained from lab experiment.

- According to the experimental results, if a broken stratum experiences both positive and negative deflections, the borehole dislocation will increase first and then decrease, approaching to its original state. As for the borehole located at the boundary of a working face, the borehole dislocation will not disappear as the overlying broken strata will experience only the positive deflection. The dislocation of the borehole wall located at the middle section of the working face will eventually vanish due to the mining-induced disturbance. Therefore, the locations of the boreholes assigned for varying purposes can be optimized.

- The observed borehole dislocation can be used to estimate the deflection and the aperture of a broken stratum and thus to assess the water conductivity of the broken stratum. The position

where borehole dislocation starts to occur corresponds to the highest breakage position of overlying strata. Larger dislocation of the borehole wall suggests greater rotation angle of the broken stratum, resulting in higher degree of conductivity. The extension height of the conductive fissures was predicted by measuring the dislocation of the surface borehole of LW8203. The prediction matched well with the in-situ observations, demonstrating the reliability of the proposed method.

Author Contributions: Jinfeng Ju and Jialin Xu conceived and designed the experiments; Jingmin Xu performed the experiments; Jinfeng Ju and Jingmin Xu analyzed the data; Jinfeng Ju wrote the paper.

Conflicts of Interest: The authors declare no conflict of interest.

References

1. Xuan, D.Y.; Xu, J.L.; Wang, B.L.; Teng, H. Borehole investigation of the effectiveness of grout injection technology on coal mine subsidence control. *Rock Mech. Rock Eng.* **2015**, *48*, 2435–2445. [CrossRef]

2. Karatela, E.; Taheri, A.; Xu, C.S.; Stevenson, G. Study on effect of in-situ stress ratio and discontinuities orientation on borehole stability in heavily fractured rocks using discrete element method. *J. Pet. Sci. Eng.* **2016**, *139*, 94–103. [CrossRef]

3. Mavko, G.; Jizba, D. Estimating grain-scale fluid effects on velocity dispersion in rocks. *Geophysics* **1991**, *56*, 1940–1949. [CrossRef]

4. Peng, S.P.; Fu, J.T.; Zhang, J.C. Borehole casing failure analysis in unconsolidated formations: A case study. *J. Pet. Sci. Eng.* **2007**, *59*, 226–238. [CrossRef]

5. Hashemi, S.S.; Taheri, A.; Melkoumian, N. An experimental study on the relationship between localised zones and borehole instability in poorly cemented sands. *J. Pet. Sci. Eng.* **2015**, *135*, 101–117. [CrossRef]

6. Ghajari, A.; Kamali, M.; Mortazavi, S.A. A comprehensive study of Laffan Shale Formation in Sirri oil fields, offshore Iran: Implications for borehole stability. *J. Pet. Sci. Eng.* **2013**, *107*, 50–56. [CrossRef]

7. Zhang, J.C. Borehole stability analysis accounting for anisotropies in drilling to weak bedding planes. *Int. J. Rock Mech. Min. Sci.* **2013**, *60*, 160–170. [CrossRef]

8. Lavrov, A.; Taghipour, A.; Ytrehus, J.D.; Mårdalen, J.; Lund, H.; Vrålstad, T.; Lund, B.; Carlsen, I.M.; Saasen, A.; Wold, S.; et al. Numerical and experimental study of the stability of non-circular boreholes in high-permeability formations. *Int. J. Rock Mech. Min. Sci.* **2014**, *68*, 128–135. [CrossRef]

9. Rahimi, R.; Nygaard, R. Comparison of rock failure criteria in predicting borehole shear failure. *Int. J. Rock Mech. Min. Sci.* **2015**, *79*, 29–40. [CrossRef]

10. Shen, J.; Jin, H.W.; Xu, J.L. Study of methane drainage borehole destruction induced by rock strata movement. *Saf. Coal Mines* **2010**, *41*, 1–4.

11. Liu, J.Z.; Sun, H.T.; Hu, Q.T. Surface borehole synthesis tension deformation fracture time-space rule. *Int. J. Rock Mech. Min. Sci.* **2012**, *22*, 465–470. [CrossRef]

12. Qian, M.G.; Miao, X.X.; Xu, J.L. Theoretical study of key stratum in ground control. *J. China Coal Soc.* **1996**, *21*, 225–230.

13. Qian, M.G.; Miao, X.X.; Xu, J.L.; Mao, X.B. *Study of Key Strata Theory in Ground Control*; China University of Mining and Technology Press: Xuzhou, China, 2003; pp. 10–15.

14. Zhu, W.B.; Xu, J.M.; Xu, J.L.; Chen, D.Y.; Shi, J.X. Pier-column backfill mining technology for controlling surface subsidence. *Int. J. Rock Mech. Min. Sci.* **2017**, *96*, 58–65. [CrossRef]

15. Xuan, D.Y.; Xu, J.L.; Zhu, W.B. Dynamic disaster control under a massive igneous sill by grouting from surface boreholes. *Int. J. Rock Mech. Min. Sci.* **2014**, *71*, 176–187. [CrossRef]

16. Qu, Q.D.; Xu, J.L.; Wu, R.L.; Qin, W.; Hu, G.Z. Three-zone characterisation of coupled strata and gas behaviour in multi-seam mining. *Int. J. Rock Mech. Min. Sci.* **2015**, *78*, 91–98. [CrossRef]

17. Ju, J.F.; Xu, J.L. Structural characteristics of key strata and strata behaviour of a fully mechanized longwall face with 7.0 m height chocks. *Int. J. Rock Mech. Min. Sci.* **2013**, *58*, 46–54. [CrossRef]

18. Miao, X.X.; Qian, M.G. Advance in key strata theory of mining rockmass. *J. China Univ. Min. Technol.* **2000**, *29*, 25–29.

19. Xu, J.L.; Qian, M.G. Method to distinguish key strata in overburden. *J. China Univ. Min. Technol.* **2000**, *29*, 463–467.

20. Li, H.C. *Similar Material Model Test of Underground Pressure*; China University of Mining and Technology Press: Xuzhou, China, 1988; pp. 63–70.

21. Huang, B.X.; Liu, C.Y.; Xu, J.L. Research on through degree of overlying strata fracture fissure induced by mining. *J. China Univ. Min. Technol.* **2010**, *39*, 45–49.